


Oxidation and phase transition in covalently functionalized MoS₂

Narine Moses Badlyan ^{1,2,*}, Nina Pettinger ¹, Niklas Enderlein ¹, Roland Gillen,¹ Xin Chen ³, Wanzheng Zhang,³ Kathrin C. Knirsch,³ Andreas Hirsch ³ and Janina Maultzsch ^{1,2}

¹Department of Physics, Friedrich-Alexander-Universität Erlangen-Nürnberg, 91058 Erlangen, Germany

²Institut für Festkörperphysik, Technische Universität Berlin, 10623 Berlin, Germany

³Department of Chemistry and Pharmacy, Friedrich-Alexander-Universität Erlangen-Nürnberg, 91058 Erlangen, Germany

 (Received 30 May 2022; revised 22 August 2022; accepted 23 August 2022; published 8 September 2022)

We present a Raman study of MoS₂ powders and MoS₂ individual layers covalently functionalized with organic molecules. In MoS₂ powders, the defect-induced “LA” Raman mode shows evidence for successful functionalization. Increasing temperature induces oxidation of both functionalized and nonfunctionalized MoS₂ into MoO₃. In contrast, mechanically exfoliated individual MoS₂ layers do not transfer into MoO₃ under the same conditions. Instead, the Raman spectra show that the procedure of covalent functionalization leads to a partial transition from the 2H into the 1T’ crystallographic phase in few-layer MoS₂. We support the identification of the 1T’ phase by DFT calculations of the corresponding vibrational modes in the mono- and bilayer 1T’-MoS₂.

DOI: [10.1103/PhysRevB.106.104103](https://doi.org/10.1103/PhysRevB.106.104103)

I. INTRODUCTION

Modifying the optical and electronic properties of two-dimensional transition metal dichalcogenides (TMDCs), such as molybdenum disulfide (MoS₂), through covalent or non-covalent functionalization has proven to be a promising approach in recent years [1–4]. Covalent functionalization has significant advantages over noncovalent functionalization, for example it enables stronger bonding between the functional groups and MoS₂, which usually leads to a better electronic communication [5]. Since covalent functionalization and oxidation affect the physical properties of TMDCs, detailed understanding of these processes is required. For analyzing the resulting modifications of the physical properties of MoS₂, Raman spectroscopy is one of the most versatile tools. It provides information on the presence of defects [6], strain [7,8], layer number [9], crystallographic structure, and electron-phonon coupling [10,11]. The so-called LA(M) Raman mode was identified as signature for defects in monolayer (1L) MoS₂ [6], thin MoS₂ layers [12], and MoS₂ nanoparticles [13]. This LA(M) mode is also detected due to disorder in the MoS₂ structure through covalent binding of functional groups. Yet, other Raman modes might be affected by the functionalization procedure as well. For example, the formation of MoO₃ in functionalized MoS₂ has been reported [1,14], but has not been explored for mechanically exfoliated MoS₂ layers. Moreover, covalent functionalization is mostly done in dispersions of chemically exfoliated MoS₂, in contrast to mechanically exfoliated individual MoS₂ layers on a substrate, which provide much better control. Hence, it is

important to understand the different effects of covalent functionalization on the physical properties of MoS₂ and related TMDCs.

Here, we present systematic investigations of MoS₂ powder before and after functionalization and of its oxidative behavior, depending on temperature and excitation laser power. The MoS₂ samples were functionalized using three different functional groups via three different chemical reactions. Regardless of the type of functional groups, all functionalized MoS₂ samples are modified by covalent C-S bonds.

Second, we analyze the influence of covalent functionalization on the Raman modes of single-layer (1L) to five-layer (5L) mechanically exfoliated MoS₂ (*me*-MoS₂) on Si/SiO₂ substrate. We show that in contrast to chemically exfoliated MoS₂ (*ce*-MoS₂) powder, *me*-MoS₂ layers do not undergo oxidation, but instead a phase transition from 2H-MoS₂ to 1T’-MoS₂, if two or more layers are used. Our findings on the 1T’ phase are supported by first-principles calculations of the phonon modes in two-layer 1T’-MoS₂. As 2H-MoS₂ and 1T’-MoS₂ are expected to have different electrical conductivity, the formation of the 1T’ phase through our covalent functionalization procedure together with methods for patterning the functionalization [15,16], open the way to create devices based on different phases within the same MoS₂ sheet.

II. METHODS

Raman experiments. The Raman spectra of MoS₂ powder samples were recorded on a Horiba LabRAM HR 800 micro-Raman setup. Micro-Raman measurements of *me*-MoS₂ on Si/SiO₂ were carried out on a Horiba LabRAM Aramis spectrometer. All measurements were performed in backscattering geometry with excitation wavelengths of 457 nm, 532 nm, or 633 nm under ambient conditions. For the temperature-dependent measurements, we used a Linkam THMS600 stage and kept the laser power below 2 Wm⁻² (1.5×10^{-3} mW) in order to avoid sample heating. All Raman spectra have been calibrated using neon lines.

*narine.mosesbadlyan@fau.de

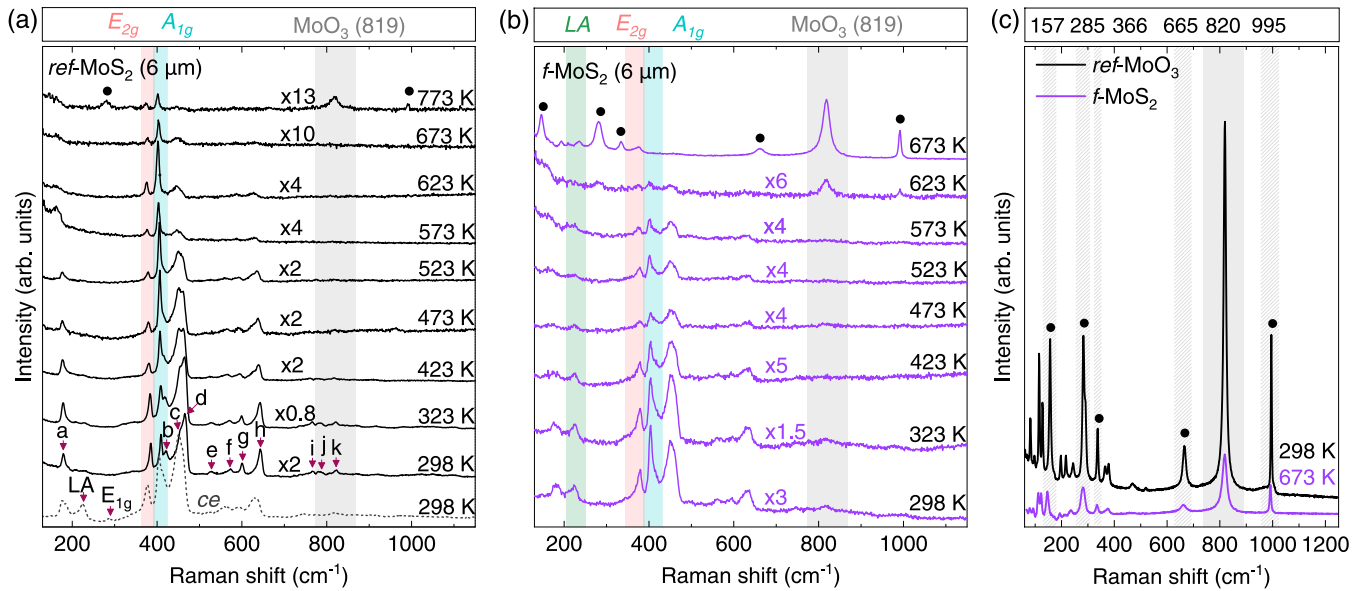


FIG. 1. Temperature-dependent Raman spectra of (a) *ref*-MoS₂ and (b) *f*-MoS₂ powder (6 μm) in the range from 298 K to 773 K. The positions of the $E_{2g}(\Gamma)$ (385 cm⁻¹) and $A_{1g}(\Gamma)$ (409 cm⁻¹) modes, the defect-induced $LA(M)$ (225 cm⁻¹) mode, and the characteristic mode of MoO₃ (819 cm⁻¹) are highlighted. Further Raman frequencies and combination modes/overtones are marked in purple arrows see also Refs. [11,25–28] and are shown in Table S1 within the Supplemental Material [24]. The black points mark less intense MoO₃ peaks. The Raman spectrum of *ce*-MoS₂ at 298 K is included for comparison (dashed line). (c) Raman spectrum of MoO₃ powder (black) at 298 K as a reference for the *f*-MoS₂ (violet) sample at 673 K. Spectra were measured with 633-nm excitation.

Computational approach. The theoretical phonon frequencies were calculated using the density functional perturbation theory (DFPT) module of Quantum Espresso [17]. A local density approximation was applied and optimized norm-conserving pseudopotentials [18,19] were used with an energy cutoff of 150 Ry. The geometry of 1L 1T'-MoS₂ was taken from Ref. [20]. Different bilayer stackings were tested; only the most stable bilayer stacking was used for the phonon calculation in this paper. Structural optimizations were performed until the residual forces acting on every atom and the cell stresses were below 0.34 meV/Å and 0.006 GPa, respectively. In out-of-plane direction, a vacuum distance of more than 16.5 Å was used to ensure that the out-of-plane interaction between periodic images of the unit cell is negligibly small. Brillouin zone integration for the calculation of the electronic ground state was carried out on a 12 × 24 × 1 (gives equal in-plane density since the 1T' structure is a 2 × 1-superstructure) electron momentum grid, whereas for the phonon calculation a 6 × 12 × 1 grid was used. A Gaussian smearing of 0.02 Ry was included.

Preparation of materials according to the reported procedures Refs. [1,14,21–23] can be found in the Supplemental Material [24].

III. RESULTS AND DISCUSSION

Figure 1 shows the temperature-dependent Raman spectra of 6-μm MoS₂ powder samples before [(a), *ref*-MoS₂] and after functionalization [(b), *f*-MoS₂] at temperatures from 298 to 773 K. For comparison, the Raman spectrum of *ce*-MoS₂, used as a precursor for chemical functionalization, is shown as a dashed line in (a). The characteristic E_{2g} and A_{1g} Raman modes of *ref*-MoS₂ at 385 cm⁻¹ and 409 cm⁻¹ correspond

to an in-plane and out-of-plane vibration, respectively [9,11]. Signatures of the second-order Raman processes and combination modes appear at higher phonon frequencies, see Table S1 within the Supplemental Material [24].

In the Raman spectrum of *f*-MoS₂, an additional mode arises at 225 cm⁻¹, which is not visible in the reference spectrum. This mode corresponds to the longitudinal acoustic LA phonon at the M point of the Brillouin zone of MoS₂ [12,29,30], which is generally forbidden for the first-order Raman scattering of MoS₂. However, in the presence of defects the $LA(M)$ mode becomes allowed, as shown in Refs. [6,31]. The Raman spectrum of *ce*-MoS₂ also displays this feature. This can be attributed to the intercalation process. The lithium intercalation induced emergence of this $LA(M)$ has been extensively studied previously [32,33]. This defect-induced $LA(M)$ mode is also found in functionalized 2-μm MoS₂ powder samples at 227 cm⁻¹ (see Fig. S3 within the Supplemental Material [24]) and in functionalized *me*-MoS₂ samples at 229 cm⁻¹, see Fig. 3(b). A similar result has been observed for MoS₂ grown by chemical vapor deposition, which was functionalized with 4-bromobenzene diazonium tetrafluoroborate [30]. In our previous study [15] we compared two functionalized *me*-MoS₂ samples prepared with activation (Na/K) and without activation. Indeed, the *me*-MoS₂ sample, which was directly functionalized without activation, showed a smaller $LA(M)$ mode. Thus, the presence of the $LA(M)$ mode can be used as an indicator for successful covalent functionalization. The overall intensities of all pristine MoS₂ (*ref*-MoS₂) Raman modes decrease with increasing temperature (298–773 K). Besides, a red shift of all Raman modes with increasing temperature is observed (cf. Fig. 1(a) and Fig. S2(b) within the Supplemental Material [24]), as reported previously [34] and expected due to lattice

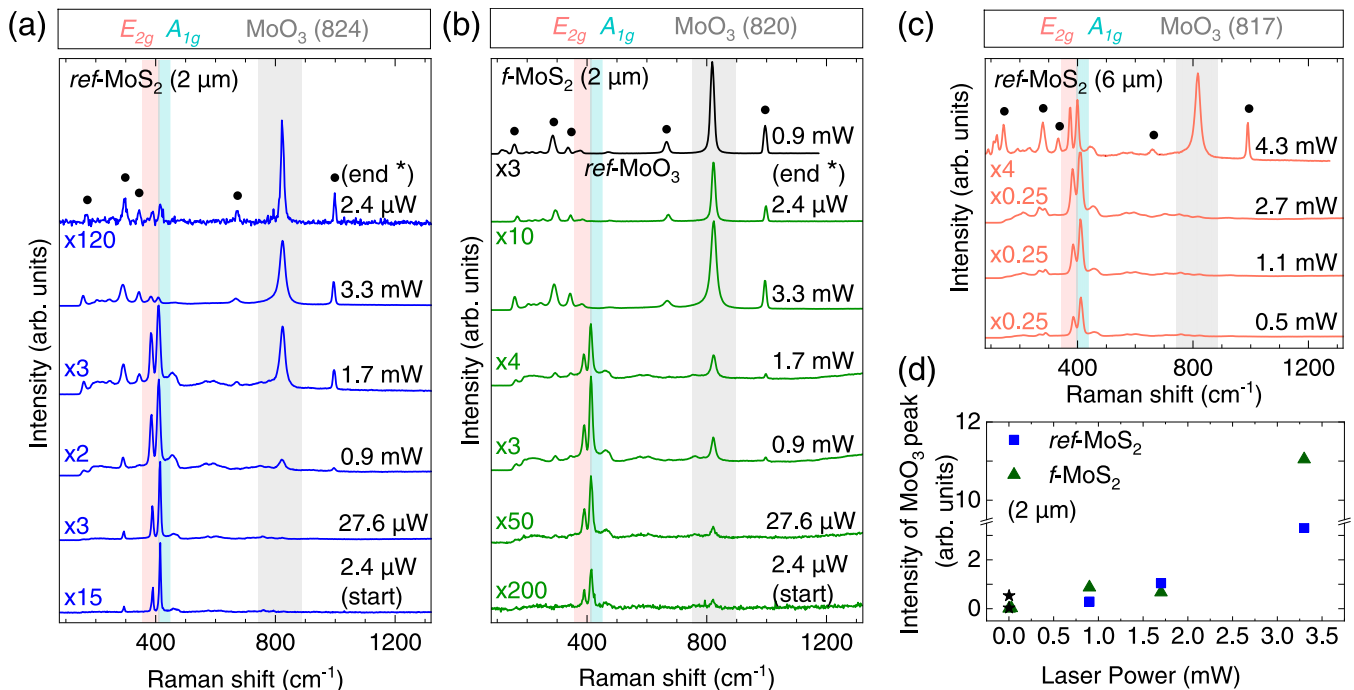


FIG. 2. Power-dependent Raman spectra of (a) *ref*-MoS₂ and (b) *f*-MoS₂ powder (2 μm) in comparison to the (c) 6 μm *ref*-MoS₂ samples. The black spectrum in (b) reflects the *ref*-MoO₃ (at 0.9 mW). The positions of the E_{2g} , A_{1g} , and MoO₃ modes are highlighted. The black points mark less intense MoO₃ peaks. The start and end of the measurement is marked with an asterisk. Spectra were recorded using an excitation wavelength of 457 nm at room temperature. Note that the $LA(M)$ mode is visible for an excitation wavelength of 633 nm and 532 nm (cf. Figs. S3, S12, and S8 within the Supplemental Material [24]) and not for 457 nm. (d) Intensity (peak area) of the MoO₃ mode at about 820 cm⁻¹ of the *ref*-MoS₂ and *f*-MoS₂ samples (2 μm) as function of laser power.

expansion. No other significant changes at temperatures below 623 K are visible. At 773 K, three additional Raman modes appear around 280, 819, and 991 cm⁻¹. In agreement with Refs. [25,35] these modes are attributed to MoO₃, indicating partial oxidation of MoS₂.

Regarding temperature-induced oxidation, the functionalized MoS₂ (*f*-MoS₂) samples show a stronger temperature dependence. At temperatures above 573 K, *f*-MoS₂ begins to oxidize to MoO₃, shown in Fig. 1(b). Between 623 K and 673 K, the *f*-MoS₂ modes disappear completely, while the intensities of the MoO₃ modes increase and become predominant, indicating a complete oxidation of MoS₂ to MoO₃ [25]. We verified our observations by measuring pristine MoO₃ powder as a reference (*ref*-MoO₃), as depicted in Fig. 1(c) and compared to the *f*-MoS₂ sample at 673 K. All peaks in the Raman spectrum of *f*-MoS₂ at this high temperature can clearly be attributed to MoO₃ modes and are in agreement with the reported literature values obtained for bulk [35]. From aryl-functionalized MoS₂, it is well known that defunctionalization of the material can occur at higher temperatures, proven by detection of the cleaved functional groups or their fragments at about 633 K [1]. Accordingly, it can be assumed that in our case, at an even higher temperature of 673 K, the arylated sample is very likely to be defunctionalized. However, a detailed understanding to what extent there is a correlation between the high degree of oxidation (Mo-O formation) and defunctionalization (C-S bond cleavage), is beyond the scope of this paper.

In samples based on 2 μm MoS₂ powder, we observe MoO₃ peaks at even lower temperatures (523 K and 423 K for 2 μm

ref-MoS₂ and 2 μm *f*-MoS₂, respectively, see Fig. S3 within the Supplemental Material [24]), i.e., the 2-μm samples are more easily being oxidized than the 6-μm samples.

A similar effect of oxidation is observed when exciting the samples at different laser powers. The power-dependent Raman spectra of (a) *ref*-MoS₂ and (b) *f*-MoS₂ powder (2 μm) are shown in Fig. 2. Again, the most intense peak (around 824 cm⁻¹ in *ref*-MoS₂ and 820 cm⁻¹ in *f*-MoS₂, cf. Fig. 2) at high laser power originates from MoO₃. In *f*-MoS₂ (2 μm) oxidation starts already at very low laser power of 2.4 μW as seen by the small MoO₃ peak. At 0.9 mW, oxidation starts also in the *ref*-MoS₂, it further increases in both samples with increasing laser power. Figure 2(d) displays the intensity of MoO₃ mode at about 820 cm⁻¹ of the *ref*-MoS₂ and *f*-MoS₂ samples as a function of laser power. We observe similar behavior for the *ref*-MoS₂ powder (6 μm), see Fig. 2(c), although the sample starts to oxidize at higher laser power (> 2.7 mW). This phenomenon reflects the relatively high stability of the *ref*-MoS₂ (6 μm) against oxidation. We repeated the power-dependent measurements with the 633 nm laser for *ref*-MoS₂ (2 μm, see Fig. S12 within the Supplemental Material [24]). We found that the measurements confirm our initial conclusion regarding the oxidation of the chemically exfoliated *ce*-MoS₂ samples, showing that this effect does not depend on the laser wavelengths used here. In contrast, no oxidation of the functionalized *me*-MoS₂ sample (see Fig. S8 within the Supplemental Material [24]) can be detected for any laser power presented here, which proves the much higher stability of the mechanically exfoliated flakes compared to the powder samples. A possible reason for the different stabilities

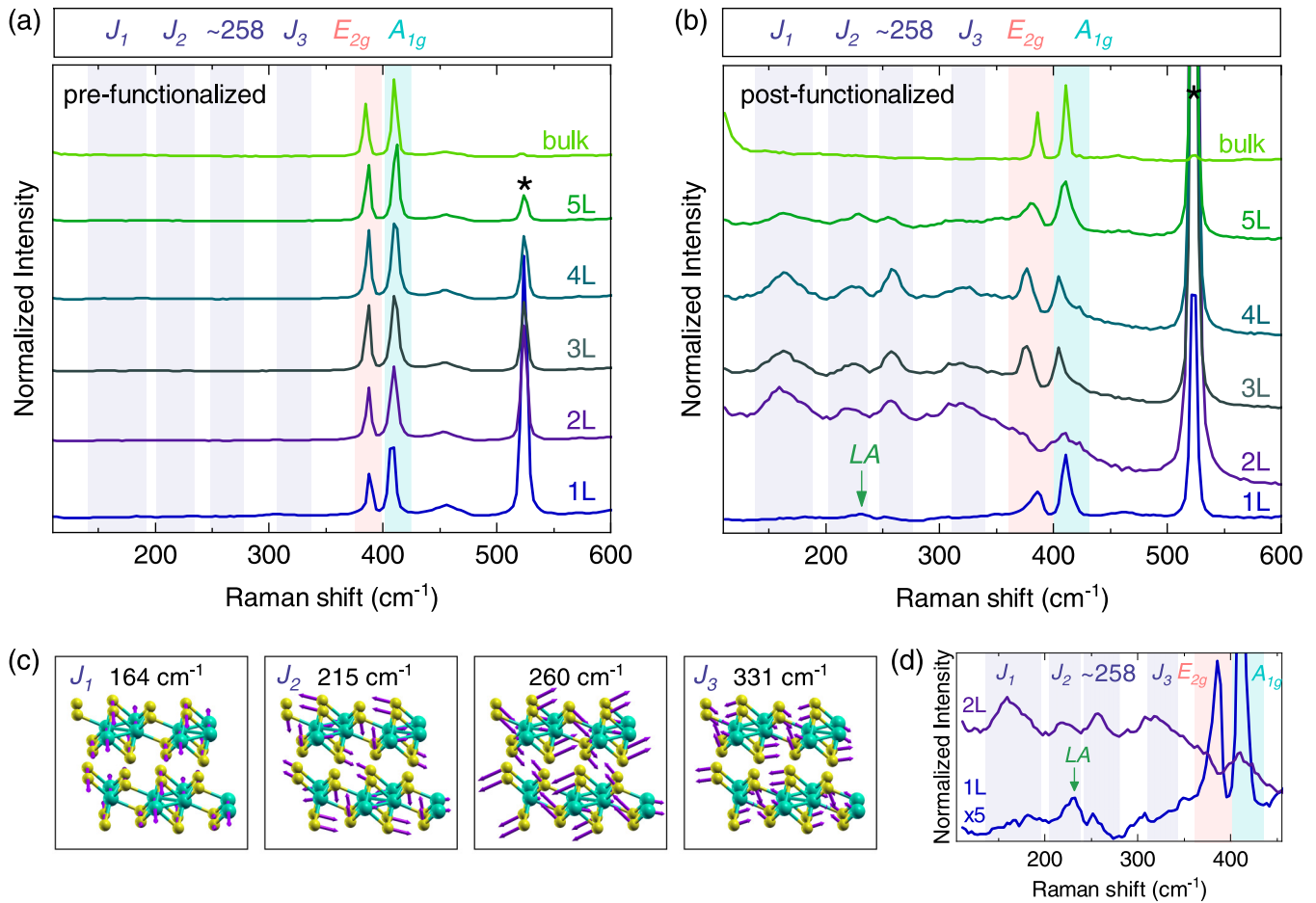


FIG. 3. Raman spectra of 1L to 5L *me*-MoS₂ before (a) and after functionalization (b). The 2L to 5L Raman spectra of the postfunctionalized material exhibit the three characteristic phonon modes J_1 , J_2 , and J_3 of the 1T'-MoS₂ phase, and an additional peak at about 258 cm⁻¹. The asterisk labels the Raman peak of the Si/SiO₂ substrate and bulk for comparison. The spectra are recorded using an excitation wavelength of 532 nm at room temperature; intensities are normalized to the A_{1g} Raman mode. (c) Computed phonon modes of 2L 1T'-MoS₂ assigned to the experimental J_1 - J_3 modes and to the Raman mode at 258 cm⁻¹; the computed phonon frequencies are indicated. The arrows indicate the displacements of the atoms. (d) Comparison between functionalized 1L and 2L *me*-MoS₂.

could be that the *me*-MoS₂ sample contains larger crystalline domains and less defects than the *ref*-MoS₂ powder samples. In general, we attribute the oxidation of the MoS₂ powder samples and the red shift of the Raman modes with increasing laser power to local temperature increase [34], which may consequently also lead to a defunctionalization of the *f*-MoS₂ material. The start and end points of the Raman measurement series in Figs. 2(a) and 2(b) and Fig. S12 within the Supplemental Material [24] show that the oxidation to MoO₃ is a nonreversible process. This is also observed in the temperature series of Fig. 1.

In order to analyze the influence of covalent functionalization on mechanically exfoliated MoS₂ samples, we investigated 1L to 5L MoS₂ on Si/SiO₂ substrate before and after functionalization. The number of layers is identified by (i) optical microscopy images (see Fig. S10 within the Supplemental Material [24]) and (ii) confirmed by the frequency difference between the E_{2g} and A_{1g} Raman modes (see Fig. S11 within the Supplemental Material [24]) [9]. Figure 3(a) shows Raman spectra of *me*-MoS₂ layers before functionalization. We did not observe noticeable differences

in the peak intensities of the E_{2g} and A_{1g} modes for different few-layer samples. In the few-layer functionalized MoS₂ layers [Fig. 3(b)], three additional modes arise at about 158 cm⁻¹, 221 cm⁻¹, and 332 cm⁻¹, corresponding to the so-called J_1 , J_2 , and J_3 modes, respectively [20,36–39]. These peaks are not observed in the monolayer samples. The presence of the J_1 - J_3 modes suggests a phase transition to the 1T' phase [20,37–39]. The 1T' phase is a distorted structure of the metallic 1T phase. Monolayer 1T'-MoS₂ has a small band gap on the order of 0.1 eV [40] and has been predicted to be a topological insulator [41]. The band gap of few-layer 1T'-MoS₂ is not known, but we expect a similar small-gap or quasimetallic behavior as in 1L 1T'-MoS₂. Yet detailed measurements would be necessary to determine the conductivity after different procedures of chemical functionalization, where also adsorbates might play a role. As we will show below, the additional, yet unassigned, peak at 258 cm⁻¹, further supports the presence of the 1T' phase. The absence of the E_{2g} mode in the spectrum of two-layer (2L) MoS₂ indicates an almost complete transition to the 1T' phase, as has been reported for freshly functionalized samples and for 1T'-MoS₂

nanosheets [36,38,39]. On the other hand, the preserved E_{2g} mode in the spectra of the other functionalized few-layer samples suggests a coexistence of the 2H and 1T' phase. For 1L MoS₂, an additional feature at 229 cm⁻¹ appears [Figs. 3(b) and 3(d)], which can be attributed to the defect-induced $LA(M)$ mode, indicating successful functionalization, similar to the case of f -MoS₂ powder. Note that this mode partially overlaps with the J_2 mode in the few-layer samples. The activation of 2H-MoS₂ with n -butyllithium (n -BuLi) leads to a charge transfer from n -BuLi to MoS₂ [1,42]. This process can cause the transition from the semiconducting 2H phase to the 1T' phase, due to the increase of the electron density located in the d orbital of Mo [42]. The absence of the J_1 - J_3 peaks and of the peak at 258 cm⁻¹ could indicate that the 1L MoS₂ does not undergo a phase transformation from 2H to 1T' during the activation process.

To support interpretation of the additional Raman modes in few-layer f -MoS₂ samples, we performed density functional theory calculations of the phonon modes in 2L 1T'-MoS₂. We find phonon modes corresponding to the J_1 , J_2 , J_3 Raman peaks at 164 cm⁻¹ (J_1), 215 cm⁻¹ (J_2), and 331 cm⁻¹ (J_3). These frequencies agree well with the experiments. Their vibrational patterns shown in Fig. 3(c) are in accordance to those of 1L 1T'-MoS₂ [20]. In 1L 1T'-MoS₂, the calculations predict also a phonon mode at 252 cm⁻¹, however it is Raman-forbidden. In contrast, in 2L 1T'-MoS₂, this mode becomes Raman-active as part of a Davydov pair. As shown by Scheuschner *et al.* [11], in general, each phonon mode of a 1L system gives rise to N modes in the corresponding N -layer system. These N -layer modes are of similar frequency (in case of weak interlayer coupling) and their vibration patterns are composed of different superpositions of the vibration pattern of the corresponding 1L mode. If the 1L layer system possesses an inversion center or a horizontal mirror plane, the N modes are attributed to two different representations of the N -layer system's symmetry group, i.e., they are either even or odd with respect to spatial inversion or mirror symmetry. Thereby, a symmetry-forbidden 1L mode can give rise to a Raman-active mode in the N -layer system with similar frequency. This phenomenon can therefore be considered as a "pseudoactivation" of the Raman-forbidden 1L mode. In our case of 2L 1T'-MoS₂, it explains the observation of the peak at 258 cm⁻¹. Its calculated frequency is 260 cm⁻¹, in excellent agreement with the experimental value of 258 cm⁻¹.

The vibration pattern is shown in Fig. 3(c), it is even under spatial inversion and therefore Raman-active.

IV. CONCLUSIONS

We have investigated the effect of oxidation and the influence of covalent functionalization on the Raman modes of powder and mechanically exfoliated MoS₂ layers. Defect-induced $LA(M)$ phonon modes are observed in the ce -MoS₂ and f -MoS₂ powders at around 225 cm⁻¹, as well as in functionalized me -MoS₂ few-layer samples at around 229 cm⁻¹. The presence of the $LA(M)$ mode in f -MoS₂ samples, independent of the type of functional groups, can be used as an indicator for the successful covalent functionalization.

Our temperature-dependent Raman measurements show the formation of MoO₃ in MoS₂ powder at elevated temperature before and after functionalization. A similar effect of oxidation is realized by increasing the laser power in a non-reversible process. In contrast, in functionalized me -MoS₂, we did not observe any oxidation effects of the functionalized layers, which reflects the high stability of this material.

For functionalized me -MoS₂ few-layer flakes, we further find evidence for the transition from the semiconducting 2H to the 1T' phase. The 1T' phase in 2L me -MoS₂ is characterized by the emergence of the three J_1 (158 cm⁻¹), J_2 (221 cm⁻¹), J_3 (332 cm⁻¹) modes, an additional peak at about 258 cm⁻¹, and the disappearance of the E_{2g} mode. The J_1 - J_3 peaks and the peak at 258 cm⁻¹ cannot be observed in 1L flakes, confirming that the 2H phase is maintained in the functionalized 1L MoS₂. The Raman spectra of 3L to 5L me -MoS₂ indicate a coexistence of the 2H and 1T' phase. Our results and identification of the 1T' phase are supported by our first-principles calculations of the phonon modes in 2L 1T'-MoS₂.

ACKNOWLEDGMENTS

This work was partly funded by the Deutsche Forschungsgemeinschaft (DFG, German Research Foundation) – Project No. 447264071 – through the SFB 953 “Synthetic Carbon Allotropes” – B13 and A1 and has received funding from the European Union's Horizon 2020 research and innovation programme Graphene Flagship under Grant Agreement No. 881603.

The authors declare no competing financial interest.

-
- [1] K. C. Knirsch, N. C. Berner, H. C. Nerl, C. S. Cucinotta, Z. Gholamvand, N. McEvoy, Z. Wang, I. Abramovic, P. Vecera, M. Halik *et al.*, *ACS Nano* **9**, 6018 (2015).
 - [2] D. Voiry, A. Goswami, R. Kappera, C. d. C. C. e Silva, D. Kaplan, T. Fujita, M. Chen, T. Asefa, and M. Chhowalla, *Nat. Chem.* **7**, 45 (2015).
 - [3] X. Chen and A. R. McDonald, *Adv. Mater.* **28**, 5738 (2016).
 - [4] R. Tilmann, C. Weiß, C. P. Cullen, L. Peters, O. Hartwig, L. Höltingen, T. Stimpel-Lindner, K. C. Knirsch, N. McEvoy, A. Hirsch, and G. S. Duesberg, *Adv. Electron. Mater.* **7**, 2000564 (2021).
 - [5] E. E. Benson, H. Zhang, S. A. Schuman, S. U. Nanayakkara, N. D. Bronstein, S. Ferrere, J. L. Blackburn, and E. M. Miller, *J. Am. Chem. Soc.* **140**, 441 (2018).
 - [6] S. Mignuzzi, A. J. Pollard, N. Bonini, B. Brennan, I. S. Gilmore, M. A. Pimenta, D. Richards, and D. Roy, *Phys. Rev. B* **91**, 195411 (2015).
 - [7] C. Rice, R. J. Young, R. Zan, U. Bangert, D. Wolverson, T. Georgiou, R. Jalil, and K. S. Novoselov, *Phys. Rev. B* **87**, 081307(R) (2013).
 - [8] A. Castellanos-Gomez, R. Roldán, E. Cappelluti, M. Buscema, F. Guinea, H. S. van der Zant, and G. A. Steele, *Nano Lett.* **13**, 5361 (2013).

- [9] C. Lee, H. Yan, L. E. Brus, T. F. Heinz, J. Hone, and S. Ryu, *ACS Nano* **4**, 2695 (2010).
- [10] S. Sarkar, I. Maity, H. L. Pradeepa, G. Nayak, L. Marty, J. Renard, J. Coraux, N. Bendiab, V. Bouchiat, S. Das, K. Majumdar, M. Jain, and A. Bid, *Phys. Rev. B* **101**, 205302 (2020).
- [11] N. Scheuschner, R. Gillen, M. Staiger, and J. Maultzsch, *Phys. Rev. B* **91**, 235409 (2015).
- [12] K. Gołasa, M. Grzeszczyk, K. P. Korona, R. Bożek, J. Binder, J. Szczytko, A. Wyszomolek, and A. Babiński, *Acta Phys. Pol., A* **124**, 849 (2013).
- [13] G. L. Frey, R. Tenne, M. J. Matthews, M. S. Dresselhaus, and G. Dresselhaus, *Phys. Rev. B* **60**, 2883 (1999).
- [14] X. Chen, C. Bartlam, V. Lloret, N. Moses Badlyan, S. Wolff, R. Gillen, T. Stimpel-Lindner, J. Maultzsch, G. Duesberg, C. K. Knirsch, and A. Hirsch, *Angew. Chem. Int. Ed.* **60**, 13484 (2021).
- [15] X. Chen, M. Kohring, M. Assebban, B. Tywoniuk, C. Bartlam, N. Moses Badlyan, J. Maultzsch, G. Duesberg, H. Weber, K. Knirsch *et al.*, *Chem. Eur. J.* **27**, 13117 (2021).
- [16] T. Dierke, D. Dasler, T. Nagel, F. Hauke, A. Hirsch, and J. Maultzsch, *ACS Appl. Nano Mater.* **5**, 4966 (2022).
- [17] P. Giannozzi, S. Baroni, N. Bonini, M. Calandra, R. Car, C. Cavazzoni, D. Ceresoli, G. L. Chiarotti, M. Cococcioni, I. Dabo *et al.*, *J. Phys.: Condens. Matter* **21**, 395502 (2009).
- [18] D. R. Hamann, *Phys. Rev. B* **88**, 085117 (2013).
- [19] M. J. van Setten, M. Giantomassi, E. Bousquet, M. J. Verstraete, D. R. Hamann, X. Gonze, and G.-M. Rignanese, *Comput. Phys. Commun.* **226**, 39 (2018).
- [20] M. Calandra, *Phys. Rev. B* **88**, 245428 (2013).
- [21] A. Castellanos-Gomez, M. Buscema, R. Molenaar, V. Singh, L. Janssen, H. S. Van Der Zant, and G. A. Steele, *2D Mater.* **1**, 011002 (2014).
- [22] X. Lefevre, O. Segut, P. Jégou, S. Palacin, and B. Jousset, *Chem. Sci.* **3**, 1662 (2012).
- [23] F. Hof, R. A. Schäfer, C. Weiss, F. Hauke, and A. Hirsch, *Chem. Eur. J.* **20**, 16644 (2014).
- [24] See Supplemental Material at <http://link.aps.org/supplemental/10.1103/PhysRevB.106.104103> for Figs. S1 and S2: illustration of the functionalization process, Raman spectra of 1L and 2L *me*-MoS₂ before and after functionalization, table of Raman frequencies *ref*-MoS₂. Figures S3 to S12: Temperature-dependent Raman spectra of *ref*-MoS₂ and *f*-MoS₂ powder (2 μm) before and after functionalization, *E*_{2g} and *A*_{1g} Raman modes as a function of laser power, power-dependent Raman spectra of functionalized *me*-MoS₂ (2H) 1L, computed phonon modes of 1L 1T'-MoS₂, optical microscopy images of *me*-MoS₂ flakes, Raman spectra for the identification of layer number, and power-dependent Raman spectra of *ref*-MoS₂ powder (2 μm).
- [25] B. C. Windom, W. Sawyer, and D. W. Hahn, *Tribol. Lett.* **42**, 301 (2011).
- [26] X. Zhang, X.-F. Qiao, W. Shi, J.-B. Wu, D.-S. Jiang, and P.-H. Tan, *Chem. Soc. Rev.* **44**, 2757 (2015).
- [27] J.-U. Lee, J. Park, Y.-W. Son, and H. Cheong, *Nanoscale* **7**, 3229 (2015).
- [28] Q. Qian, Z. Zhang, and K. J. Chen, *Phys. Rev. B* **97**, 165409 (2018).
- [29] H. Tornatzky, R. Gillen, H. Uchiyama, and J. Maultzsch, *Phys. Rev. B* **99**, 144309 (2019).
- [30] Y. Park, S. Shin, Y. An, J.-G. Ahn, G. Shin, C. Ahn, J. Bang, J. Baik, Y. Kim, J. Jung, and H. Lim, *ACS Appl. Mater. Interfaces* **12**, 40870 (2020).
- [31] H. Guo, Y. Sun, P. Zhai, J. Zeng, S. Zhang, P. Hu, H. Yao, J. Duan, M. Hou, and J. Liu, *Nucl. Instrum. Methods Phys. Res., Sect. B* **381**, 1 (2016).
- [32] S. J. R. Tan, I. Abdelwahab, Z. Ding, X. Zhao, T. Yang, G. Z. J. Loke, H. Lin, I. Verzhbitskiy, S. M. Poh, H. Xu *et al.*, *J. Am. Chem. Soc.* **139**, 2504 (2017).
- [33] S. Park, C. Kim, S. O. Park, N. K. Oh, U. Kim, J. Lee, J. Seo, Y. Yang, H. Y. Lim, S. K. Kwak *et al.*, *Adv. Mater.* **32**, 2001889 (2020).
- [34] S. Sahoo, A. P. Gaur, M. Ahmadi, M. J.-F. Guinel, and R. S. Katiyar, *J. Phys. Chem. C* **117**, 9042 (2013).
- [35] M. Py and K. Maschke, *Phys. B: Condens. Matter* **105**, 370 (1981).
- [36] S. Jiménez Sandoval, D. Yang, R. F. Frindt, and J. C. Irwin, *Phys. Rev. B* **44**, 3955 (1991).
- [37] A. P. Nayak, T. Pandey, D. Voiry, J. Liu, S. T. Moran, A. Sharma, C. Tan, C.-H. Chen, L.-J. Li, M. Chhowalla *et al.*, *Nano Lett.* **15**, 346 (2015).
- [38] C. Guo, J. Pan, H. Li, T. Lin, P. Liu, C. Song, D. Wang, G. Mu, X. Lai, H. Zhang *et al.*, *J. Mater. Chem. C* **5**, 10855 (2017).
- [39] X. Fan, P. Xu, D. Zhou, Y. Sun, Y. C. Li, M. A. T. Nguyen, M. Terrones, and T. E. Mallouk, *Nano Lett.* **15**, 5956 (2015).
- [40] X. Yin, Q. Wang, L. Cao, C. S. Tang, X. Luo, Y. Zheng, L. M. Wong, S. J. Wang, S. Y. Quek, W. Zhang, A. Rusydi, and A. T. S. Wee, *Nat. Commun.* **8**, 486 (2017).
- [41] X. Qian, J. Liu, L. Fu, and J. Li, *Science* **346**, 1344 (2014).
- [42] D. Voiry, A. Mohite, and M. Chhowalla, *Chem. Soc. Rev.* **44**, 2702 (2015).